



Ministry of Science, Research & Technology
Iranian Research Organization
for Science and Technology

Research paper

The effect of nanoclay on the creation of clusters of polyamide 6 microfibrils

Roya Mashayekhi¹, Morteza Ehsani^{1,2,*}, Shervin Ahmadi², Ramin Khajavi¹, Hossein Ali Khonakdar²

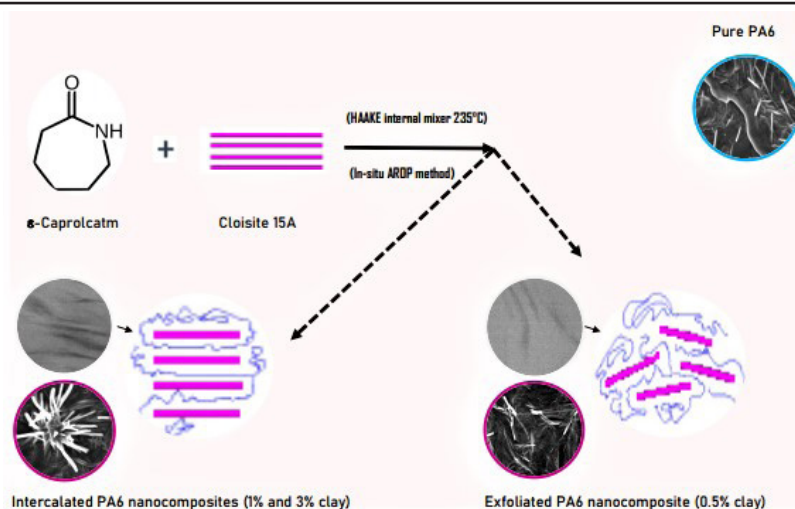
¹ Polymer and Textile Department, Islamic Azad University, South Tehran Branch, Tehran, Iran

² Iran Polymer and Petrochemical Institute (IPPI), Tehran, Iran

HIGHLIGHTS

- In the PA6/clay nanocomposite (0.5 % nanoclay), the nanoparticles were exfoliated.
- In the PA6/clay nanocomposites (1 and 3% nanoclay), the particles were intercalated.
- The PA6/clay nanocomposite showed a pseudo-solid behavior.
- The clay-centered PA6 microfibrils clustering during AROP has not been reported before.
- The clusters of PA6 microfibrils formed whose growth from the nanoclay.

GRAPHICAL ABSTRACT



ARTICLE INFO

Article history:

Received 21 October 2022

Revised 23 November 2022

Accepted 27 November 2022

Keywords:

Polyamide 6

Nanoclay

Nanocomposites

Clusters

In-situ polymerization

ABSTRACT

The PA6/clay nanocomposites were prepared during *in-situ* anionic ring-opening polymerization (AROP) via reactive melt blending in a Hake internal mixer. Then, the samples were characterized using FT-IR, DSC, DMTA, rheometer, XRD, SEM/EDX/elemental mapping, TEM, and HT-GPC to study the effects of Cloisite 15A on PA6 properties. The results showed that nanoclay caused a decrease in the ultimate tensile strength (UTS), crystallinity, T_m , T_g , and $\tan \delta$ of the samples. However, it increased the Young's modulus and stress rupture of the samples. Furthermore, the nanocomposites showed a pseudo-solid behavior because of the reinforcing effect of the nanoparticles. Additionally, α crystals were not seen in the samples with 1 % and 3 % nanoclay; however, γ crystals were observable in those samples. Also, nanoclay decreased PA6 viscosity and increased dispersity and residual monomers in the nanocomposite samples. The nanoclays exfoliated in the sample have 0.5 % nanoparticles, but they were intercalated by more loading in the PA6 matrix. Moreover, the PA6 microfibrils were observed as sporadic and clay-centered clusters in the SEM micrographs of the pure and nanocomposite samples, respectively. Therefore, the clustering of PA6 microfibrils in the matrix during *in-situ* AROP is considered a novelty in current research.

* Corresponding author: Tel.: +9821-44787091 ; Fax: +9821-44787096 ; E-mail address: m.ehsani@ippi.ac.ir

DOI: 10.22104/JPST.2022.5914.1216

1. Introduction

Polyamide 6 (PA6) is an engineering plastic [1] that can be applied in electrical devices [2], semiconductors, photocatalysts [3], biomedical devices [4], the packaging industry [5], the automotive industry [6], coatings, textiles [7], nanofiber-reinforced composites, and high-performance plastics [8,9]. In addition, some of PA6 advantages are proper self-lubrication [10], high service temperature, chemical resistance [11], high corrosion resistance [12], stiffness [13], proper strength [14], manufacturability [15], water absorption, bending, thermal conductivity properties [16], readily tailored properties [17], easy to wash, high durability [18], and low price [19].

PA6 is a semi-crystalline polymer consisting of two main phases α and γ . The extent of each phase depends on factors like the presence of nanoparticles in the matrix and processing conditions [1]. The α crystals have hydrogen bonding (H-bonding) between non-parallel chains, and the γ crystal has H-bonding between parallel chains. The H-bonding in the α crystal is stronger than in the γ crystal. Therefore, the α crystal is more stable than the γ crystal [10]. It is worth noting that the polar end groups of PA6, including carboxyl (C=O) and amino (–N–H), are all reactive under certain conditions [2]. They can cause ion-dipole and dipole-dipole interactions and form H-bonding [9,19].

Usually, the PA6 synthesis starts with the ring-opening polymerization (ROP) process of the ϵ -caprolactam (CL) [2] and continues via one of the hydrolytic, anionic, or cationic polymerization methods. Cationic ring-opening polymerization (CROP) is not applicable to any industry due to the product's low molecular weight (MW) [20]. However, the use of two methods, anionic ring-opening polymerization (AROP) and hydrolytic ring-opening polymerization (HROP), are prevalent in the industrial production of PA6 [21]. The AROP method has advantages over the HROP due to the high degree of high MW, crystallization (X_c), the possibility of reaction under the melting point (T_m), and a shorter reaction time. Considering that using hazardous solvents in the industrial production of polymers is one reason for environmental pollution, selecting this method for producing PA6 would be helpful because it is performed without any solvent [20].

Generally, AROP activators are divided into two categories of chemical structure: acyl-lactams and

isocyanates [22]. Furthermore, organometallic reagents such as alkaline and other potassium and sodium compounds are used as AROP initiators [12,20]. Sodium caprolactamate (NaCL) is the most widespread initiator of *in-situ* polymerization of caprolactam [1]. AROP in the presence of hexamethylene diisocyanate (HDI) and NaCL reduces the length of PA6 chains in the γ crystals [23].

Several drawbacks, such as low-dimensional stability, high moisture absorption, and low thermal degradation, limit the usage of PA6 [24,25]. Industrial PA6 generally consists of linear chains and exhibits low melt strength, which restricts its usage in the blowing, spinning, and foaming processes [26]. Accordingly, the strength of PA6 can be improved significantly by many chemical modifying strategies such as adding nanoparticles, branching, crosslinking, and chain extension [13].

However, branched chains affect the processing and rheological behaviors of polymers [27]. Nanoparticles can improve PA6 properties such as electrical, thermal, optical [5], mechanical [14], barrier properties, and durability [13,18]. They are usually added to polymers because of their unique properties, such as sensing, magnetic hyperthermia, therapeutic, and non-toxicity [21,29], and are more effective in polymer properties in relatively low amounts due to the large aspect ratio [30,31]. The preparation of nanocomposites depends on the aspect ratio, size, orientation, specific surface area, volume fraction used, dispersion [1,7], and compatibility of nanoparticles with the polymer matrix. In addition, the reaction rate, time, and temperature of the preparation affect the nanocomposite [32].

In addition, the *in-situ* polymerization can be affected by the interaction between the nanoparticle and the PA6 matrix and physical and mechanical properties [25], morphology, and the size of nanoparticles [13,24,33].

In recent years, inorganic nanoparticles such as CuO, NiO, MgO, SiO₂, TiO₂ [34,35], carbon nanotubes, graphene, and nanoclays [13,28] have been used for PA6 nanocomposite [26].

The PA6/clay nanocomposites are important in industrial applications because of their improved mechanical, barrier gas [7], thermal [13,36], rheological [37,38], readily tailored properties [17], and flame retardance [13,34,39] compared to conventional PA6 [31,40,41]. Nanoclay or layered silicate has an average surface area of 800 m².g⁻¹, while other nanoparticles usually have a surface area of 100 m².g⁻¹ [42]. Other

advantages include the low cost, high aspect ratio [5], proper dispersion/distribution in a matrix [43], high dimensional stability [44], low gas permeability [45], and also radiation and changing interaction with light in polymers [7,13,46]. In addition, nanoclay is applied for thermoplastics, elastomers, and thermosets [7,46,47].

The PA6/clay nanocomposite was prepared for the first time using the *in-situ* polymerization method in 1989 to manufacture timing belt housings [7] by Toyota Central R&D Labs., Inc. [7,28].

Nanoclay must be well delaminated in the polymer matrix to improve the properties of the polymers [17]. Generally, depending on the reaction between nanoclay and polymer, the silicate layers can be in one of the following situations: intercalation, ordered exfoliation, or disordered exfoliation [41]. In an intercalated system, silicate layers are swelled, and polymer chains are placed between the sheets. Therefore, the layers stack at distances of a few nanometers. In an exfoliated system, no interaction occurs between sheets at some points, so they move separately [42,48]. The exfoliation of nanoclay requires high temperatures or other external forces [48,49], and the clay modification, the processing conditions, and the matrix type affect it [5]. Also, nanoclay can be exfoliated in the PA6 matrix due to the polar end groups and H-bonding in the PA6 structure [50].

In this work, PA6/clay nanocomposites were prepared during *in-situ* AROP polymerization to investigate the effect of the nanoclay (Cloisite 15A) on their properties. First, the nanocomposites were synthesized in the presence of the nanoclay and HDI. Then, the samples were characterized by Fourier transform infrared (FT-IR) and energy-dispersive X-ray (EDX or EDS). In addition, differential scanning calorimetry (DSC), dynamic mechanical thermal analysis (DMTA), and a tensile testing machine were applied to study thermal and mechanical properties. Next, the rheological behavior of the samples was investigated using a rheometer. In addition, the samples were studied by X-ray diffractometer (XRD), transmission electron microscopy (TEM), scanning electron microscope (SEM), and elemental mapping to investigate the crystal phases and morphological properties. Also, the molecular weight (number average molecular weight (M_n)) and the weight average molecular weight (M_w)) were analyzed by gel permeation chromatography (GPC).

The clustering of the PA6 microfibrils in the matrix during *in-situ* AROP is considered a novelty in the current study.

2. Materials and methods

2.1. Materials

ϵ -Caprolactam monomer (CL, purity 99.9 %) was prepared from BASF (Germany). The nanoclay (Cloisite 15A) (polymerization grade, 99.9 %) was purchased from the Southern Clay Company (USA). Commercial PA6 (Akulon® F-236) as a control sample was prepared from DSM (Germany). Sodium caprolactam (NaCL, purity 99.9 %) as an initiator and hexamethylene diisocyanate (HDI, purity ≥ 99 %) as an activator were purchased from Merck (Germany).

2.2. Synthesis of PA6/clay nanocomposites

Specific amounts of the CL monomer were mixed with the nanoclay in the presence of NaCL as an initiator and HDI as a bi-functional activator in a HAAKE internal mixer at 235 °C for 15 min through *in-situ* AROP. The ratio of the sample's components is mentioned in Table 1.

2.3. Characterizations

The chemical structure of the powdered samples was characterized by FT-IR spectroscopy (Equinox 55, Bruker, Germany) at a resolution of 4 cm^{-1} over a wavenumber region from 4000 to 600 cm^{-1} resolution at 16 mm.s^{-1} at room temperature.

An SEM (Mira-III, Tescan, Czechia) was applied for the morphological study of the cross-section of samples. First, the samples were gold coated in a Palaron sputtering apparatus. Then, SEM-generated X-rays were collected

Table 1. The ratio of components of the samples.

Sample	CL (w/w %)	HDI (%)	NaCL (%)	Cloisite 15A
C-C	100	0	0	0
C-0	96	2	2	0
C-0.5	95.5	2	2	0.5
C-1	95	2	2	1.0
C-3	93	2	2	3.0

using the EDX (Mira-II, Tescan, Czechia). In addition, the presence of Na and Si elements was investigated by element mapping (Mira-II, Tescan, Czechia).

An XRD test of the samples was performed by a D5000 instrument (Siemens, Germany) for a total time of 20 min and a step.scan⁻¹ of 0.02 at 1.2 degrees.min⁻¹, 40 mA, and 40 kV. The data was collected from 15° to 30° (2θ). Before testing, the extraction of residual monomers was performed by immersion in distilled water for 14 h at 100 °C. Lastly, they were dried in a vacuum for 48 h at 80 °C.

The samples were cut with less than 60 nm for TEM analyses using an RMC Power tome CRX microtome. The imaging of cross-sections of the samples was performed with a Philips CM200 TEM (Germany) at an acceleration voltage of 100 kV.

The rheological behaviors of the samples were studied by a Rheoplus rheometer (MCR 501, Anton Paar, Austria). The sample sheets (4 cm × 4 cm) were heated at 240 °C for 1 min under an N₂ atmosphere. Before measurement, they were dried at 80 °C for 3 h in a vacuum oven and then kept in a desiccator [51].

The samples (5-10 mg) were characterized by DSC (STAR SW 12.00 DSC, TOLEDO METTLER, Switzerland) at a rate of 20 °C.min⁻¹ from 23 to 300 °C in standard aluminum sample pans. The heat of fusion of 100 % crystalline PA6 was considered 241 J.g⁻¹ [52].

The loss factor (tan δ) was the samples obtained by STAR[®] SW14.00 DMTA (METTLER, Switzerland). They were heated at a rate of 5 °C.min⁻¹ at a frequency of 1.00 Hz from 23 to 200 °C under an N₂ atmosphere. Then, they were dried for 48 h at 80 °C in a vacuum before measurement.

The samples' M_n , M_w , and dispersity (D) were obtained by an HLC-801A HT-GPC (TOSOH, Japan). The samples were, therefore, first solved in 1,3-cresol, then filtered through a 0.45 mm filter. Then, they were injected into GPC and measured at 240 °C.

Residual monomers of the samples were measured via the gravimetry method. First, unreacted CL monomers and low molecular weight oligomers were extracted by Soxhlet distilled water and Irganox1010 (1 wt %) at 120 °C. Then, they were dried in a vacuum oven at 80 °C for 4 h [53]. After that, their weight loss was measured as the number of residual monomers.

Tensile was measured in a universal testing machine (Instron 5584) with a 1KN load cell, standard grips, and Merlin software according to the standard ASTM

D-638 at a constant strain (10 mm.min⁻¹). In addition, the notched Izod impact of the samples was performed using Zwick according to ASTM D-256 638 at a uniform strain rate of 10 mm.min⁻¹.

3. Results and discussion

The rheological behaviors of the samples at 240 °C in an internal mixer were investigated with a torque rheometer. The evolution of torque values for the reactive melt of the samples with a constant shear rate was shown by a torque-time rheogram in Fig. 1. The figure shows that the evolution of the torque increased in C-0.5 and other samples after 5 and 7 min, respectively. Then, it decreased in the C-0, C-0.5, and C-1 samples at the 11th minute and the C-3 sample at the 12th minute. These results showed that the polymerization process in C-0.5 started faster than in the other samples; however, it took longer than theirs. However, the polymerization time of all samples was short (8-9 min) due to the *in-situ* AROP method.

Furthermore, the maximum torque amount in the C-0.5 sample was more than in the C-0 sample because loading 0.5 % nanoclay did not affect its polymerization process; it only acted as a thickener. However, in the C-1 and C-3 samples, the maximum and final torque amounts decreased compared to C-0 because the nanoclay played the role of an inhibitor.

3.1. FT-IR Spectroscopy

The FT-IR results in Fig. 2 showed no absorption band

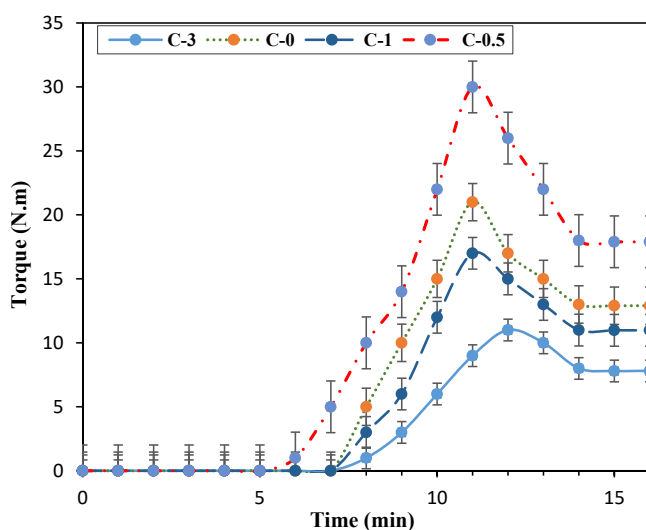


Fig. 1. Evolution of the torque vs. reaction time during the polymerization of ϵ -caprolactam in a Haake internal mixer.

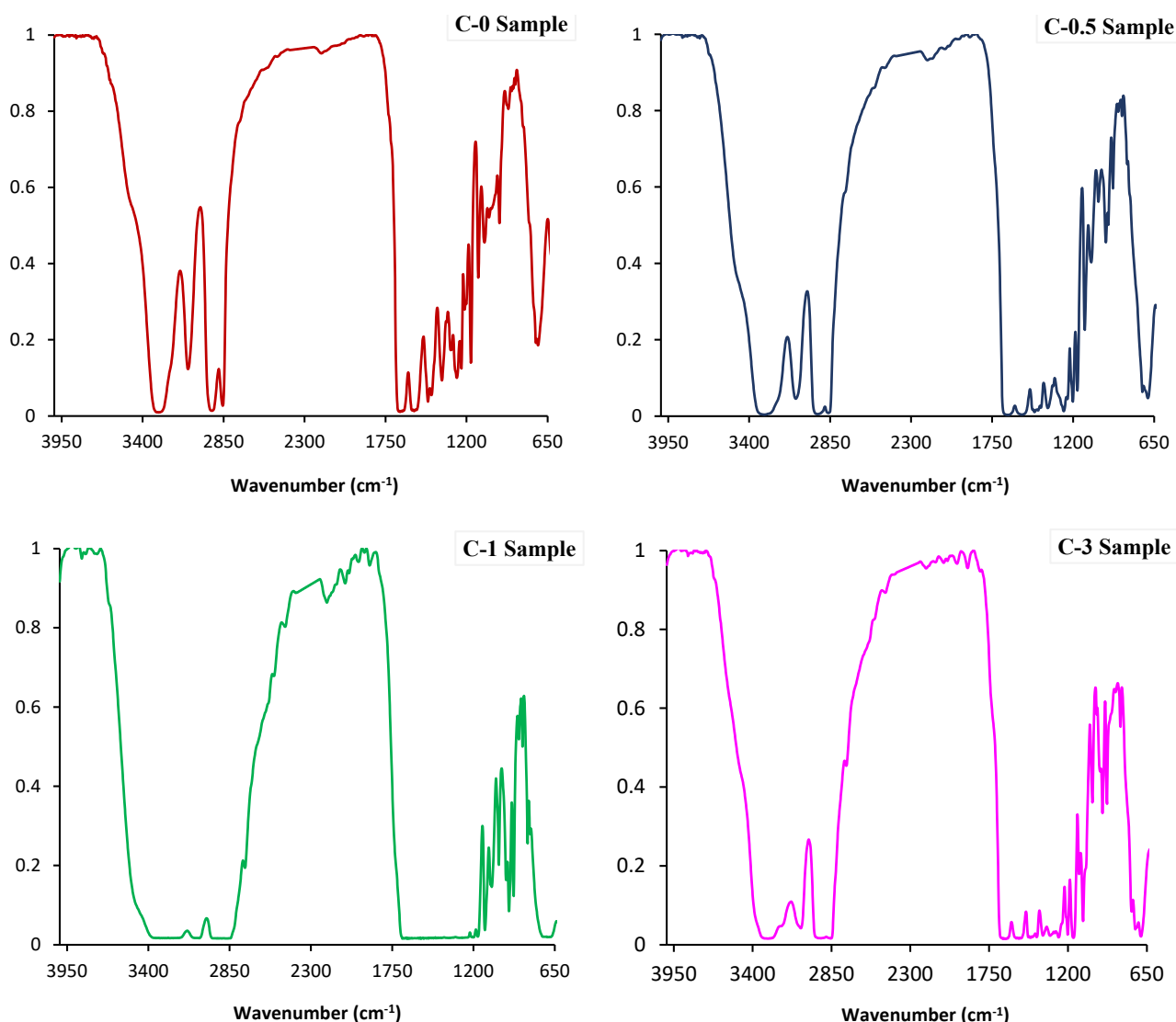


Fig. 2. The FT-IR spectra of the samples C-0, C-0.5, C-1 and C-3.

corresponding to the stretching vibration of isocyanate groups ($\text{N}=\text{C}=\text{O}$) in the samples due to the reaction of HDI with nanoparticles and CL. In addition, in the C-0 sample, the absorption bands at about 2931 cm^{-1} belonged to (C-H) stretching vibration, and at about 1261 and 1463 cm^{-1} belonged to (C-H) bending vibration; however, they shifted to about 2927 cm^{-1} for (C-H) stretching vibration and at about 1201 and 1460 cm^{-1} for (C-H) bending vibration in the nanocomposites due to the presence of clay. Moreover, the absorption bands at about 1634 and 3270 cm^{-1} belonged to (C=O) stretching vibration in the nanocomposites, and at about 1639 and 3293 cm^{-1} belonged to (C=O) stretching vibration in the C-0 sample.

Additionally, an absorption band was observed at 1097 cm^{-1} in all the nanocomposites, and its absorption percentage increased as the nanoclay amount in the polymer increased. Furthermore, two peaks were

detected at about 3062 cm^{-1} for (N-H) in all samples due to the completed polymerization process and participation of HDI in reaction with CL and nanoclay. Moreover, the absorption bands at about 3293 and 3068 cm^{-1} belonged to (N-H) stretching in the crystalline and amorphous phases of all samples, respectively [13]. These results agreed with previous research [54-56].

3.2. Thermal behavior study

The effect of the nanoclay on the thermal properties of the samples was studied by DSC. As seen in Table 2, the melting temperature (T_m) of the nanocomposites shifted lower with increasing amounts of nanoclay. Furthermore, the crystallinity percentage (X_c) of the nanocomposites decreased compared to the C-0 sample. The creation of the nanoclay-centered clusters of PA6 microfibrils and the nucleating property of

Table 2. The DSC results of the samples.

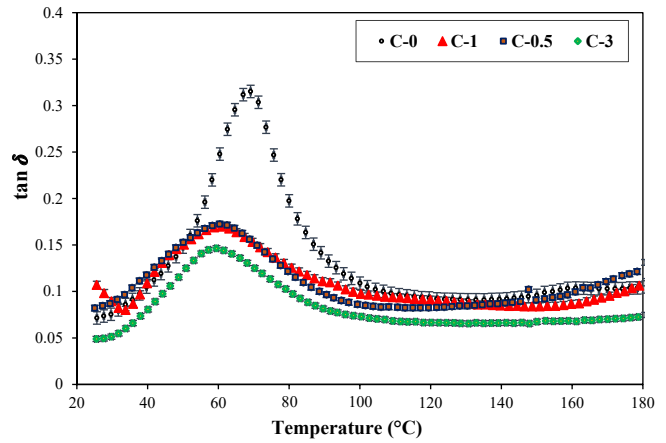
Sample	T_m (°C)	ΔH_m (J.g ⁻¹)	X_c (%)
C-0	219.36 (± 1.01)	138.44 (± 1.33)	57.4 (± 0.1)
C-0.5	215.40 (± 1.20)	128.02 (± 1.78)	53.1 (± 0.6)
C-1	211.78 (± 1.31)	74.20 (± 2.02)	30.7 (± 0.7)
C-3	206.15 (± 2.1)	53.57 (± 1.1)	22.2 (± 1.1)

the nanoclay (as a hetero-structure). In other words, nanoclays were the nucleation centers and partially prevented the homogenous crystallization of PA6 [57]. It seems that decreasing the amount of X_c in these samples decreased the glass transition temperature (T_g) due to more amorphous and a decrease in the number of H-bonding in the nanocomposites. Moreover, the melting enthalpy (ΔH_m) of the nanocomposite samples was smaller than the C-0 sample due to the reduction of crystal dimensions [57]. This study also showed that nanoclays, as nucleating agents, could change the crystallinity in the polymers [22]. These results were confirmed by the XRD and DMTA results.

3.3. DMTA analysis

Based on Fig. 3, adding the nanoclay to the samples caused a decrease in their loss factor ($\tan \delta = E''/E'$). However, a significant difference in the $\tan \delta$ values was not observed in the nanocomposite samples. Also, increasing nanoclay decreased the area under the curve (AUC) of the $\tan \delta$ peaks. The figure shows that the PA6/clay nanocomposite movement chains in the amorphous region are more than pure PA6. The free volume of sections of the side chains and small groups increases this motion in different directions and decreases $\tan \delta$ [59]. Additionally, the $\tan \delta$ in the polymers is directly related to the motion of the sections, which could be attributed to the increased plasticization effect [60,61]. Furthermore, Fig.3 showed that the maximum $\tan \delta$ of the nanocomposite samples shifted to a lower temperature than the C-0 sample. Therefore, the composite samples had a lower viscosity. Accordingly, the value of T_g in the nanocomposites was lower than in the C-0 sample due to increased PA6 chain mobility following the presence of rigid nanoparticles [13]. This is consistent with the results of other reports [62].

Moreover, it is necessary to mention that the T_g values obtained from TGA and DMTA analyses of the samples did not match. This is due to the DMTA results

**Fig. 3.** The $\tan \delta$ vs. temperature results for the samples.

being more accurate than the TGA because the effect of oscillating frequency on polymers, frequency effect changes molecular relaxations of polymer chains, and T_g behavior is considered.

3.4. Mechanical Properties

Evaluating the effect of nanoclay on the mechanical properties of the samples was performed by mechanical testing. Based on Table 3, the ultimate tensile strength (UTS) amounts of PA6/clay nanocomposites were slightly decreased due to adding nanoclay to the matrix. In other words, adding nanoparticles to the polymers reduced their crystallinity and, as a result, reduced their UTS amounts. In addition, the stress rupture and Young's modulus amounts increased without significant loss of impact resistance due to nanoclay. Studies showed that nanoclay affects the mechanical properties of short and semi-aligned fiber-reinforced PA6 composites due to its aspect ratio [8,48].

3.5. Rheological behavior

The Rheoplus rheometer was used to study the rheological behaviors of the samples. Plots of the

Table 3. The results of mechanical testing of the samples.

Sample	Impact resistance with a notch (KJ/M2)	Tensile Properties		
		UTS (%)	Stress rupture (Mpa)	Young's modulus (Mpa)
C-0	13.20 (± 0.32)	90.0 (± 0.3)	75.0 (± 0.3)	1100 (± 2)
C-0.5	13.07 (± 0.32)	87.0 (± 0.4)	80.0 (± 0.4)	1550 (± 3)
C-1	12.92 (± 0.23)	75.0 (± 0.2)	92.0 (± 0.2)	1630 (± 2)
C-3	12.85 (± 0.13)	65.0 (± 0.4)	98.0 (± 0.1)	1870 (± 4)

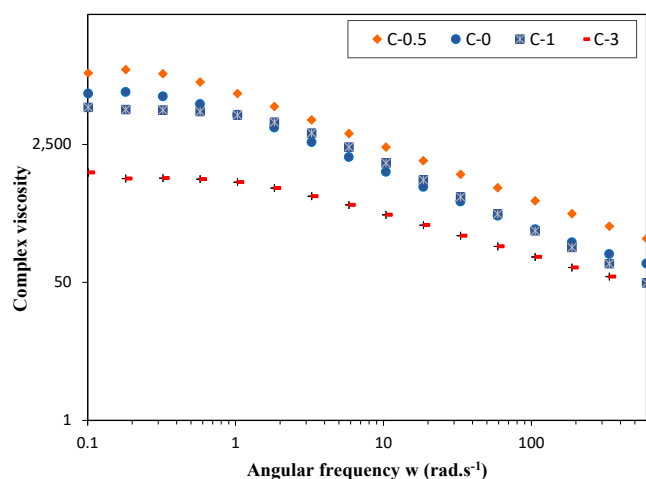


Fig. 4. Complex viscosity vs. angular frequency curves for the samples.

samples' complex viscosity vs. angular frequency are observable in Fig. 4. The figure shows that the slope of the curves decreased in the low-frequency viscoelastic range due to the presence of nanoclay. This could indicate that the reinforcing effect of nanoclay on the PA6 internal structure caused the prepared nanocomposites to show a pseudo-solid behavior because of the reinforcing effect of the nanoclay on the internal structure of polymers. Therefore, they tended to form three-dimensional superstructures such as clustered polymers [63].

The results also showed that the C-0.5 and C-3 samples had the highest and lowest zero shear viscosity, respectively. It seems that the dropping viscosity amounts in the C-1 and C-3 samples were related to the formation of clusters of PA6 microfibrils. Others have also reported that the interaction nature, the chemical structure of polymers (such as crosslinking and branching), the components of nanoparticles, and the MW affect rheological behaviors [64]. The TEM results in this study confirmed it. It is essential to mention that this allows for polymerization processability at lower temperatures and pressures [6].

3.6. XRD analysis

XRD analysis was performed in ranges of 2θ from 1° to 10° and 15° to 30° . Based on Fig. 5, the Cloisite 15A had two peaks at 2.65° and 7.16° , which indicates the distance between the adjacent nanoclay lamellar structures. Also, no peak was observed in the C-0 and C-0.5 samples. Because the C-0 sample had no nanoparticles, exfoliation of nanoparticles was completed in the C-0.5 sample. Moreover, the peak at

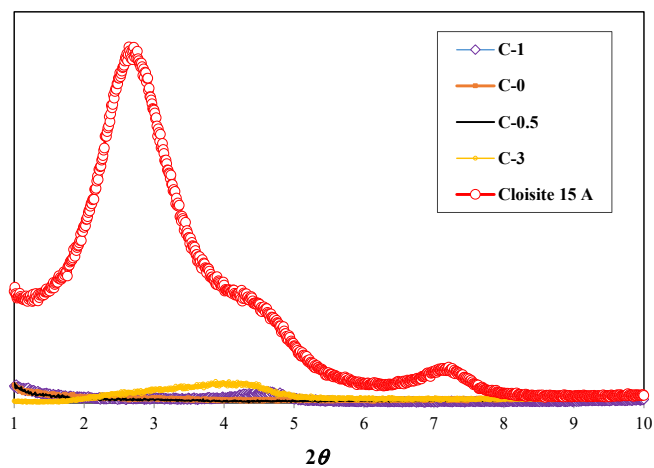


Fig. 5. X-ray diffraction (XRD) integrated patterns of the samples ($10^\circ > 2\theta$).

2.65° disappeared in the nanocomposites. Also, there were peaks at 4.44° and 4.71° in the curves of the C-1 and C-3 samples, respectively. This could be because increasing nanoparticles in the matrix only caused the intercalation of nanoparticles. In addition, the intensity of the peaks in the nanocomposites was related to increasing nanoclay content. Furthermore, based on the XRD results (Fig. 6), α_1 and α_2 crystals of the C-0 sample were observed at 20.10° and 24.04° , respectively. Also, α_1 and α_2 crystals of the C-0.5 sample shifted to 20.82° and 23.89° , respectively, and a γ crystal peak was observed at 21.61° . However, the C-1 and C-3 samples only had a single peak of γ form at 21.29° and 21.37° , respectively, due to increasing nanoclay content. It seems that the presence of nanoclay in the PA6 samples had a heterophase nucleation effect favorable for forming γ crystals due to a direct reaction between the nanoclay and the CL, followed by the creation of defects in the PA6 crystals [10]. In other words, the nanoparticles significantly affected the crystallization of the polymer

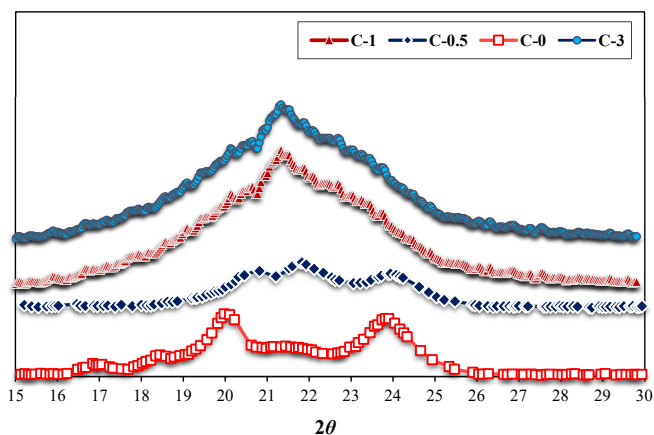


Fig. 6. XRD results of PA6/clay nanocomposite samples ($30^\circ > 2\theta > 15^\circ$).

by increasing the length of polar bonds inside the crystal and γ absorption. This can be due to a decrease in chain mobility or an increase in chain end groups in samples with lower molecular mass and more nanoparticles [55]. Another article showed that branching could increase the plasticizing properties of polymers by increasing free volume and mobility in the polymer [65].

3.7. Morphological studies

In this study, SEM, EDX/elemental mapping, and TEM analysis were used to examine the morphology of the samples. Based on SEM micrographs in Fig. 7, PA6 microfibrils were found in all samples. In the C-0

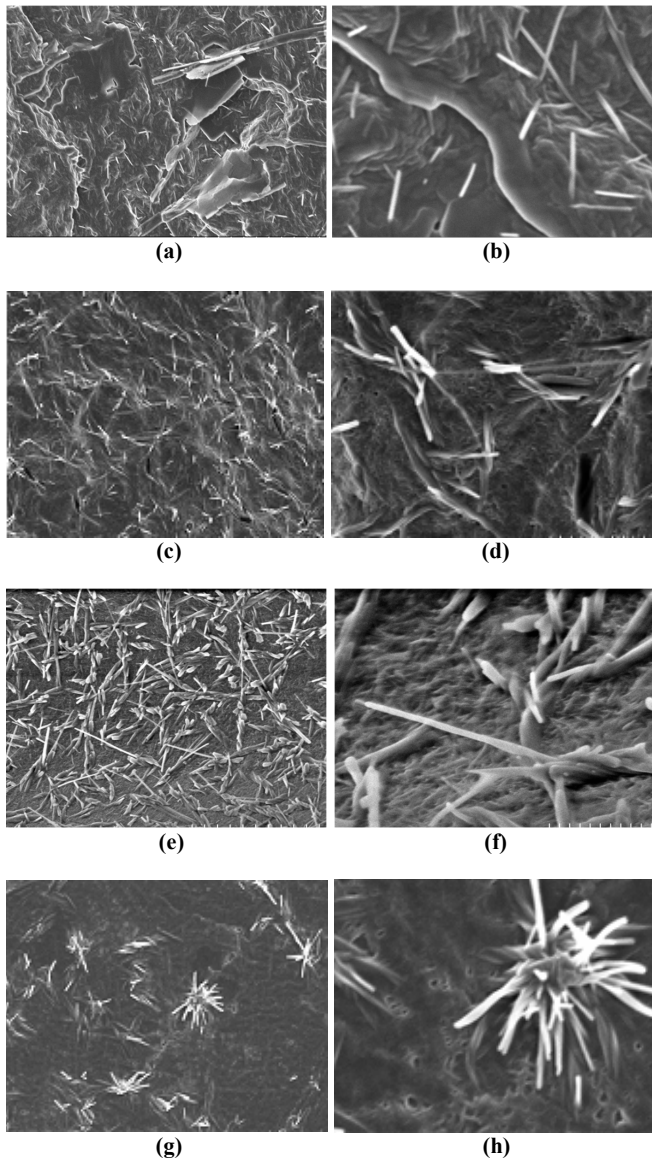


Fig. 7. SEM micrographs of the cross-section of the samples: (a) C-0 (50 KX), (b) C-0 (100 KX), (c) C-0.5 (50 KX), (d) C-0.5 (100 KX), (e) C-1 (50 KX), (f) C-1 (100 KX), (g) C-3 (50 KX), and (h) C-3(100 KX).

sample, the sporadic microfibrils were dispersed, but in the nanocomposite samples, they were observed as clay-centered clusters. Furthermore, the micrographs showed that the number and density of clusters in the nanocomposites increased as the nanoparticles increased. So, the C-3 sample had the most and densest cluster compared to the other samples.

Moreover, zooming on two points of interface between a microfibril cluster and the surface of the matrix shows that the growth of clusters of the PA6 microfibrillar began at the nanoclay surface (Fig. 8). It should be noted that the creation of clusters of PA6 microfibrils in the matrix during *in-situ* AROP has not been observed in another study before.

The dispersion of Si elements in the samples was investigated by elemental mapping. In Fig. 9, Si was observed in the center of the clusters of the PA6

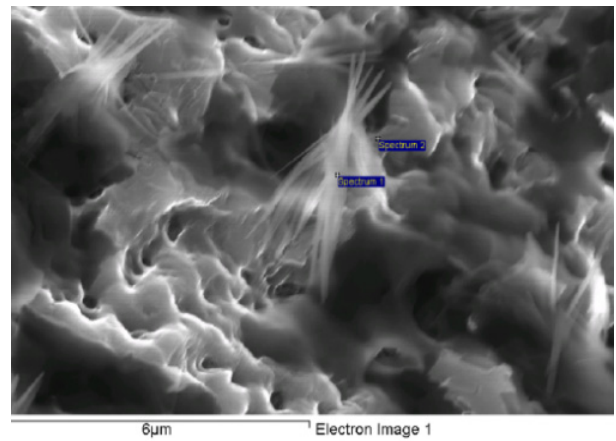


Fig. 8. SEM image of a PA6/clay nanocomposite sample.

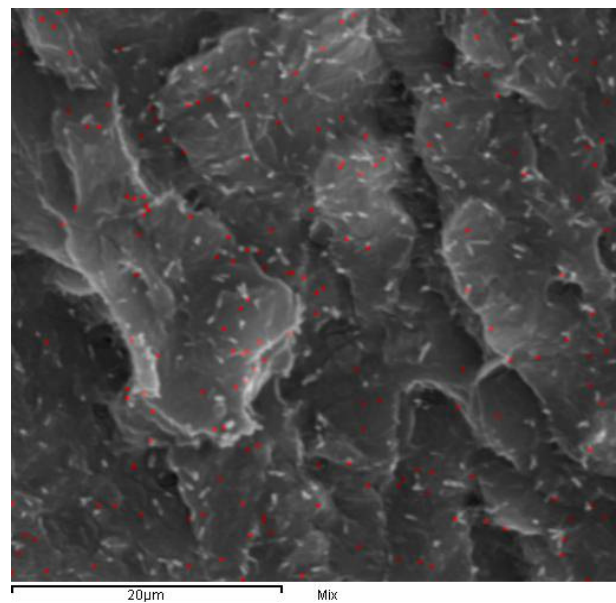


Fig. 9. Dispersion of Na of Cloisite 15A in the PA6 matrix at 200 μm magnification.

microfibrils in the nanocomposite. The XRD and DSC results showed that this structure could have a γ crystal shape.

In this research, the quantitative EDX showed Na and Si elements in the structure of all nanocomposite samples (Table 4). However, as expected, the percentage of Si increased, and the percentage of Na decreased as the nanoparticles increased, confirming the reaction of nanoclay with CL monomers. Moreover, in the C-0 sample, only Na was observed in the matrix because NaCL was in its preparation process (AROP); however, in the C-C sample, there were no Na and Si because of HROP.

Table 4. The EDX results of the samples.

Sample	C-C	C-0	C-0.5	C-1	C-3
Si (%)	0.00	0.00	17.80	25.44	43.81
Na (%)	0.00	100	82.20	74.56	56.19

Based on the TEM micrographs (Fig. 10), after adding nanoclay to the polymer, nanoclay sheets were observable in the images. In the image of the C-0.5 sample, the nanoclay sheets were inconspicuous, probably because of complete nanoclay exfoliation. However, in the images of samples C-1 and C-3, the sheets were darker and denser than in the other samples. This may be due to intercalation occurring as the amount of nanoclay increased in these samples.

3.8. GPC analysis

The HT-GPC results in Table 5 showed that the D amount increased in the nanocomposite samples after

Table 5. Comparison of the HT-GPC results of the samples.

Sample	M_w (g.mol ⁻¹)	M_n (g.mol ⁻¹)	D (M_w/M_n)
C-0	54900	50800	1.08
C-0.5	50540	46400	1.09
C-1	48800	43930	1.11
C-3	55400	49000	1.13

adding nanoclay. In addition, nanoclay reduced M_w and M_n in the prepared nanocomposites. These results confirmed the DSC, DMTA, and other analyses.

3.9. Determination of residual monomers

There are several methods for measuring the residual monomer and oligomer contents [22]. In this study, the gravimetric method was applied to measure them in the samples. As observed in Table 6, the residual monomers increased by increasing the nanoclay to the polymer ratio. These results are in agreement with the DMTA results. It seems that this was the effect of the reduction of T_g , crystallization temperature (T_c), and the resistance of the polymer as plasticizers via increased molecular motion [66].

Table 6. Residual monomer content of the samples.

Sample	Residual monomer (%)
C-0	0.1 (\pm 0.04)
C-0.5	0.3 (\pm 0.05)
C-1	0.9 (\pm 0.05)
C-3	1.8 (\pm 0.03)

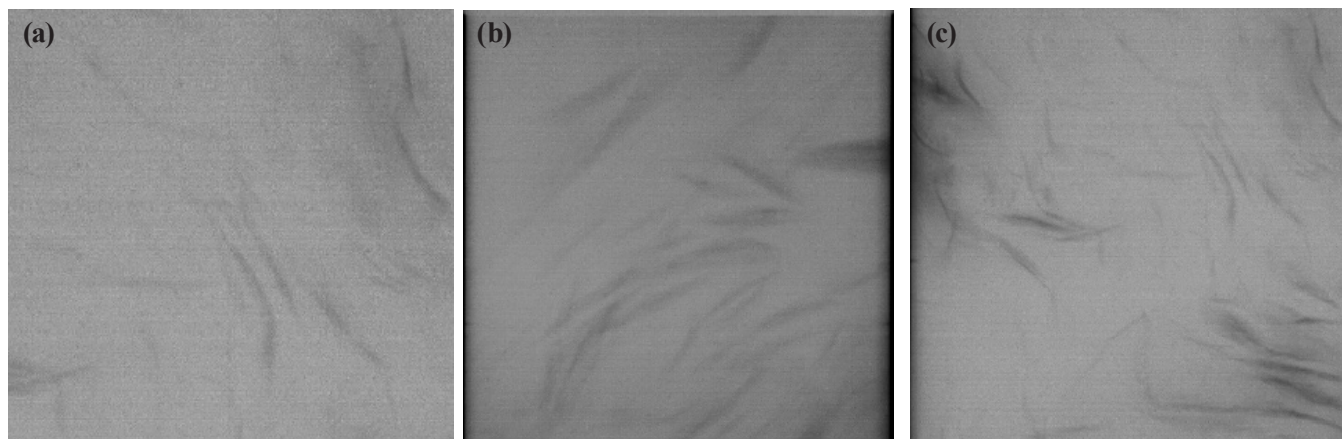


Fig. 10. TEM micrograph of the PA6/clay nanocomposite samples at a magnification of 200 nm: (a) C-0.5, (b) C-1, and (c) C-3.

4. Conclusions

The PA6/clay nanocomposite samples were prepared during *in-situ* AROP in the presence of nanoclay and HDI via reactive melt blending. Then, samples were characterized to investigate the effect of nanoclay on the properties of the synthesized nanocomposites. The results showed that the polymers' crystallinity and ΔH_m decreased due to the nucleating property of the nanoclay and the reduction of crystal dimensions, respectively. Nanoclay decreased UTS, T_g , T_m , and $\tan \delta$ amounts in the samples; however, it increased the stress rupture and Young's modulus. In addition, the reinforcing effect of the nanoparticles caused a pseudo-solid behavior in the nanocomposite. Moreover, γ crystals were observable in the samples with 1 % and 3 % nanoparticles. The nanoclay also reduced MW and viscosity and increased D and the residual monomers in the nanocomposite samples.

Test results showed that the nanoparticles were exfoliated in the sample containing 0.5 % nanoclay and were intercalated in the samples with 1 and 3 % nanoclay. Furthermore, the nanocomposites showed a pseudo-solid behavior because of the reinforcing effect of the nanoparticles. PA6 microfibrils were dispersed individually in the bulk of the pure sample, but clusters of PA6 microfibrils, whose growth started from the nanoclay surfaces, were formed in the nanocomposites. It should be noted that the formation of the clay-centered clusters of PA6 microfibrils in the matrix during *in-situ* AROP had not been reported before.

References

- [1] Pramoda, K., and Liu, T. (2004). Effect of moisture on the dynamic mechanical relaxation of polyamide-6/clay nanocomposites. *J. Polym. Sci. Pol. Phys.* 42(10)1823-1830.
- [2] Xu, M., Chen, Y., Liu, T., Zhao, L., & Park, C.B. (2019). Determination of modified polyamide 6's foaming windows by bubble growth simulations based on rheological measurements. *J. Appl. Polym. Sci.* 136(42) 48138.
- [3] Guo, F., Aryana, S., Han, Y., & Jiao, Y. (2018). A review of the synthesis and applications of polymer-nanoclay composites. *Appl. Sci.* 8(9) 1696.
- [4] Khaimov, V., Kohse, S., Arbeiter, D., Grabow, N., Schmitz, K.P. (2018). Nanofibrous polyamide 6 scaffolds promote adhesion of endothelial cells. *Biomed. Eng.* 4(1) 637-640.
- [5] Hammami, I., Hammami, H., Soulestin, J., Arous, M., & Kallel, A. (2019). Thermal and dielectric behavior of polyamide-6/clay nanocomposites. *Mater. Chem. Phys.* 232, 99-108.
- [6] Ghanta, T.S., Aparna, S., Verma, N., & Purnima, D. (2020). Review on nano- and microfilter-based polyamide 6 hybrid composite: Effect on mechanical properties and morphology. *Polym. Eng. Sci.* 60(8) 1717-1759.
- [7] Gupta, B., Lacrampe, M.F., & Krawczak P. (2006). Polyamide-6/clay nanocomposites: A critical review. *Polym. Polym. Comp.* 14(1) 13-3.
- [8] Alonso-Montemayor, F.J., Tarrés, Q., Oliver-Ortega, H., Espinach, F.X., Idalia Narro-Céspedes, R., Castañeda-Facio, A.O., & Delgado-Aguilar, M. (2020). Enhancing the mechanical performance of bleached hemp fibers reinforced polyamide 6 composites: A competitive alternative to commodity composites. *Polymers-Basel*, 12(5) 1041.
- [9] Holec, P., Jirkovec, R., Kalous, T., Bařka, O., Brořek, J., & Chvojka, J. (2022). The potential for the direct and alternating current-driven electrospinning of polyamides. *Nanomaterials-Basel*, 12(4), 665.
- [10] Xu, M., Lu, J., Qiao, Y., Wei, L., Liua, T., Lee, P.C., Zhao, L., & Park, C.B. (2020). Toughening mechanism of long-chain branched polyamide 6. *Mater. Design*, 196, 109173.
- [11] Xu, M., Lu, J., Zhao, J., Wei, L., Liu, T., Zhao, L., & Park, C.B. (2021). Rheological and foaming behaviors of long-chain branched polyamide 6 with controlled branch length. *Polymer*, 224, 123730.
- [12] Zhang X., and Loo, L.S. (2008). Morphology and mechanical properties of a novel amorphous polyamide/nanoclay nanocomposite. *J. Polym. Sci. Pol. Phys.* 46(23) 2605-2617.
- [13] Baniasadi, H., Trifol, J., Ranta, A., & Seppala, J. (2021). Exfoliated clay nanocomposites of renewable long-chain aliphatic polyamide through *in-situ* polymerization. *Compos. Part B-Eng.* 211, 108655.
- [14] Mahmud, M.B., Anstey, A., Shaayegan, V., Lee, P.C., & Park, C.B. (2020). Enhancing the mechanical performance of PA6 based composites by altering their crystallization and rheological behavior via *in-situ* generated PPS nanofibrils. *Compos. Part B-Eng.* 195, 108067.
- [15] Krasinskyi, V., Suberlyak, O., Sikor, J., &

- Zemke, V. (2021). Nanocomposites based on polyamide-6 and montmorillonite intercalated with polyvinylpyrrolidone. *Polym. Plast. Technol. Mater.* 60(15) 1641-1655.
- [16] Sakai, T., Shamsudim, N.S., Fukushima, R., & Kageyama, K. (2021) Effect of matrix crystallinity of carbon fiber reinforced polyamide 6 on static bending properties. *Adv. Compos. Mater.* 30(2) 71-84.
- [17] Chen, Y., Waghmare, P.R., & Ayranci, C. (2019). Fabrication and characterization of electrospun mats of nylon 6/silica nanocomposite fibers. *J. Eng. Fiber. Fabr.* 14, doi:10.1177/1558925019843225.
- [18] Choi, J., Shin, T., Song, K., Seo, Y. P., & Seo, Y. (2020). Nonisothermal crystallization behaviors of structure-modified polyamides (Nylon 6s). *ACS Omega*, 5(45) 29325-29332.
- [19] Zhang T. and Kang, H.J. (2021). Enhancement of the processability and properties of nylon 6 by blending with polyketone. *Polymers-Basel*, 13(19) 3403.
- [20] Cai, L., Lin, Z., & Qian, H. (2010). Dispersion of nano-silica in monomer casting nylon6 and its effect on the structure and properties of composites. *Express Polym. Lett.* 4(7) 397-403.
- [21] Nuyken O. and Pask, S.D. (2013). Ring-opening polymerization - An introductory review. *Polymers-Basel*, 5(2) 361-403.
- [22] Peter, C., LeBaron, P.C., Wang, Z., & Pinnavaia, T.J. (1999). Polymer-layered silicate nanocomposites: An overview. *Appl. Clay Sci.* 15(1-2) 11-29.
- [23] Fornes, T. and Paul, D.R. (2003). Crystallization behavior of nylon 6 nanocomposites. *Polymer*, 44(14) 3945-3961.
- [24] Ding, W., Zhou, Y., Wang, W., & Wang, J. (2020) The reactive compatibilization of montmorillonite for immiscible anionic polyamide 6/polystyrene blends via *in-situ* polymerization. *Polym.-Plast. Technol. Mater.* 59(8) 1-11.
- [25] Kausar, A. (2022). Polyamide/nanosilica nanocomposite: A chronicle of design and high-tech progressions. *Mater. Res. Innov.* 26(22) 52-63.
- [26] Khanyile, N. (2022). Advances in nanostructured polyamide-based chemical sensors. *J. Nanomater.* 2022, 5543283.
- [27] Münstedt, H. (2021). Rheological measurements and structural analysis of polymeric materials. *Polymers-Basel*, 13(7) 1123.
- [28] Morimune-Moriya, S., Yada, S. I., Kuroki, N., Ito, S., Hashimoto, T., & Nishino, T. (2020). Strong reinforcement effects of nanodiamond on mechanical and thermal properties of polyamide 66. *Comp. Sci. Technol.* 199, 108356.
- [29] Fabia, J., Gawłowski, A., Rom, M., Slusarczyk, C., Brzozowska-Stanuch, A., & Sieradzka, M. (2020). PET Fibers modified with cloisite nanoclay. *Polymers-Basel*, 12(4) 774.
- [30] Shanmugan, S., Gorjian, S., Elsheikh, A.H., Essa, F.A., Omara, Z.M., & Raghu, A.V. (2021). Investigation into the effects of SiO₂/TiO₂ nanolayer on the thermal performance of solar box type cooker. *Energ. Source. Part A*, 43(21) 2724-2737.
- [31] Lincoln, D.M., Vaia, R.A., Wang, Z.G., & Hsiao, B.S. (2001). Secondary structure and elevated temperature crystallite morphology of nylon-6/layered silicate nanocomposites. *Polymer*, 42(4) 1621-1631.
- [32] El-Gabry, L.K., Nasr, M.F., & Abou El-Kheir, A.A. (2020). A new economical technique for dyeing polyamide fiber/nanoclay composite with basic dye. *Res. J. Text. Appar.* 25(1) 47-63.
- [33] Yang, M., Gao, Y., & Li, H.M. (2007). Preparation of polyamide 6/silica nanocomposites from silica surface initiated ring-opening anionic polymerization. *Express Polym. Lett.* 1(7) 433-442.
- [34] Chen, J., Beake, B.D., Bell, G.A., Tait Y., & Gao, F. (2016). Investigation of the nanomechanical properties of nylon 6 and nylon 6/clay nanocomposites at sub-ambient temperatures. *J. Exp. Nanosci.* 11(9) 695-706.
- [35] Li, Y., Liu, K., & Xiao, R. (2017). Preparation and characterization of flame-retarded polyamide 66 with melamine cyanurate by *in-situ* polymerization. *Macromol. Res.* 25(8) 779-785.
- [36] Wu, H., Krifa, M., & Koo, J.H. (2014). Flame retardant polyamide 6/nanoclay/ intumescent nanocomposite fibers through electrospinning. *Text. Res. J.* 84(10) 1-13.
- [37] Abdel Alim Sadik, W., Maghraby El Demerdash, A.G., Abbas, R., & Bedir, A. (2020). Impact of hybrid nanosilica and nanoclay on the properties of palm rachis-reinforced recycled linear low-density polyethylene composites. *J. Thermoplast. Compos.* 35(11) 2032-2051.
- [38] Nagy D., & Kókai, E. (2018). Polymer-based nanocomposites with nanoclay. *IOP Conf. Ser.-Mat. Sci.* 448, 012021.

- [39] Li, Q., Gao, D., Wei, Q., Ge, M., Liu, W., Wang, L., & Hu, K. (2010). Thermal stability and crystalline of electrospun polyamide 6/organomontmorillonite nanofibers. *J. Appl. Polym. Sci.* 117(3) 1572-1577.
- [40] Kanapitsas, A., Pissis, P., & Kotsilkov, R. (2002). Dielectric studies of molecular mobility and phase morphology in polymer-layered silicate nanocomposites. *J. Non-Cryst. Solids*, 305, 204-211.
- [41] Koo, C.M., Kim, S.O., & Chung, I.J. (2003). Study on morphology evolution, orientational behavior, and anisotropic phase formation of highly filled polymer-layered silicate nanocomposites. *Macromolecules*, 36(8) 2748-2757.
- [42] Hanemann, T., & Szabó, D.V. (2010). Polymer-nanoparticle composites: from synthesis to modern applications. *Materials*, 3(6) 3468-3517.
- [43] Abdelwahab, M., Codou, A., Anstey, A., Mohanty, A.K., & Misra, M. (2020). Studies on the dimensional stability and mechanical properties of nanobiocomposites from polyamide 6-filled with biocarbon and nanoclay hybrid systems. *Compos. Part A- Appl. Sci.* 129, 105695.
- [44] Siddique, S., Leung, P.S., & Njuguna, J. (2021). Drilling oil-based mud waste as a resource for raw materials: A case study on clays reclamation and their application as fillers in polyamide 6 composites. *Upstream Oil Gas Technol.* 7, 100036.
- [45] Gill, Y.Q., Abid, U., & Song, M. (2020). High performance nylon12/clay nanocomposites for potential packaging applications. *J. Appl. Polym. Sci.* 137(41) 49247.
- [46] Mekhroum, M.E.M., Raji, M., Rodrigue, D., El Kacem Qaissa, A., & Bouhfid, R. (2020). The effect of benzothiazolium surfactant modified montmorillonite content on the properties of polyamide 6 nanocomposites. *Appl. Clay Sci.* 185, 105417.
- [47] Tuna, B., & Benkreira, H. (2019). Chain extension of polyamide 6/organoclay nanocomposites. *Polym. Eng. Sci.* 59(6) 1233-1241.
- [48] Krishnamoorti, R., & Yurekli, K. (2001). Rheology of polymer layered silicate nanocomposites. *Curr. Opin. Colloid In.* 6(5-6) 464-470.
- [49] Kakuta, T., Baba, Y., Yamagishi, T.A., & Ogoshi, T. (2021). Supramolecular exfoliation of layer silicate clay by novel cationic Pillar[5]arene intercalants. *Sci. Rep.-UK*, 11, 10637.
- [50] Saha, M., Ray, R., Choudhury, A.R., De Bhowmik, P., & Kumar Ballabh, T. (2021). Impact of exfoliation/intercalation of nano-clay on structure, morphology and electrical properties of poly(ethylene oxide) based solid nanocomposite electrolytes. *J. Polym. Res.* 28(8) 299.
- [51] Ruymbeke, E.V., Slot, J.J.M., Kapnistos, M., & PAM, S. (2013) Structure and rheology of branched polyamide 6 polymers from their reaction recipe. *Soft Matter*, 9(29) 6921-6935.
- [52] Anisio da Paz, R., Melissa, A., Leite, D., Maria Araújo, E., da Medeiros, V.N., Jeferson de Melo, T.A., & Pessan, L.A. (2016). Mechanical and thermomechanical properties of polyamide 6/ brazilian organoclay nanocomposites. *Polímeros*, 26(1) 52-60.
- [53] Ehsan, K. Y. A., Avramenko, V., & Ahmadi, S. (2013). Reducing the flammability of nylon-6 by introducing a fireproofing agent during the anionic polymerization of ϵ -caprolactam. *Int. Polym. Sci. Technol.* 40(9) 19-21.
- [54] Li, L., & Yang, G. (2009). Synthesis and properties of hydroxyapatite nanorod-reinforced polyamide 6 nanocomposites. *Polym. Int.* 58(4) 380-387.
- [55] Xu, Q., Chen, F., Li, X., & Zhang, Z. (2013). The effect of surface functional groups of nanosilica on the properties of polyamide 6/SiO₂ nanocomposite. *Poli. J. Chem. Technol.* 15(3) 20-24.
- [56] Sar, P., Ghosh Roy, S., De, P., & Ghosh S. (2020). Synthesis of glutamic acid derived organogels and their applications in dye removal from aqueous medium. *Macromol. Mater. Eng.* 305(4) 1900809.
- [57] Zanoag, M., Airinei, A., Fifer, N., Grigoras, C.V., Țîmpu, D., & Tanasa, F. (2021). Critical assessment of structural changes in some co-polyamide-clay hybrid materials in correlation with the filler characteristics. *Polym. Compos.* 42(11) 5936-5951.
- [58] Zhang, S., Zhang, J., Tang, L., Huang, J., Fang, Y., Ji, P., Wang, C., & Wang, H. (2019). A novel synthetic strategy for preparing polyamide 6 (PA6)-based polymer with transesterification. *Polymers-Basel*, 11(6) 978.
- [59] Vasanthan, N., & Salem, D. (2001). FTIR Spectroscopic characterization of structural changes in polyamide 6 fibers during annealing and drawing. *J. Polym. Sci. Pol. Phys.* 39(5) 536-547.
- [60] Geethamma, V. G., Asaletha, R., Kalarikkal, N., & Thomas, S. (2014). Vibration and sound damping in polymers. *Resonance*, 19, 821-833.

- [61] Kiziltas, E., Yang, H. S., & Kiziltas, A., Boran, S., Douglas, E., & Gardner, J. (2016). Thermal analysis of polyamide 6 composites filled by natural fiber blend. *Bioresources*, 11(2) 4758-4769.
- [62] Hutchinson, J. M. (2009). Determination of the glass transition temperature. Methods correlation and structural heterogeneity. *J. Therm. Anal. Calorim.* 98, 579-589.
- [63] Reyhani, R., Zadhoush, A., Salman Tabrizi, N., Nazockdašt, H., & Naeimirad, M.R. (2021). The influence of CNT-doped carbon aerogels on microstructural, rheological and mechanical properties of epoxy nanocomposites. *Compos. Sci. Technol.* 215, 109031.
- [64] Taghizadeh, E., Naderi, G., & Dubois, C. (2010). Rheological and morphological properties of PA6/ECO nanocomposites. *Rheol. Acta* 49, 1015-1027.
- [65] Han, Y.K., Um, J.W., Im, S.S., & Kim, B.C. (2001). Synthesis and characterization of high molecular weight branched PBA. *J. Polym. Sci. Pol. Chem.* 39(13) 2143-2150.
- [66] Gad, M.M., Rahoma, A., & Al-Thobity, A.M. (2018). Effect of polymerization technique and glass fiber addition on the surface roughness and hardness of PMMA denture base material. *Dent. Mater. J.* 37(5) 746-753.